Cell, Volume *129*

Supplemental Data

Intercellular Coupling Confers Robustness against Mutations in the SCN Circadian Clock Network

Andrew C. Liu, David K. Welsh, Caroline H. Ko, Hien G. Tran, Eric E. Zhang, Aaron A. Priest, Ethan D. Buhr, Oded Singer, Kirsten Meeker, Inder M. Verma, Francis J. Doyle III, Joseph S. Takahashi, and Steve A. Kay

Genotype	Behavior [a]	SCN Explants	Individual SCN Neurons [b]	Lung Explants [c]	Fibroblasts [c]	Individual Fibroblasts [b]
Cry+/+	**23.52±0.11 (n=8)**	**24.41±0.39 (n=5)**	**27.23±2.44 (n=106)**	**23.70±0.35 (n=7)**	**25.88±0.75 (n=8)**	**24.63±1.13 (n=16)**
Cry1-/-	**22.82±0.11 (n=6)**	**22.53±0.69 (n=6)**	**AR/ND (n=7)**	**AR/ND (n=6)**	**AR/ND (n=5)**	**AR/ND (n=6)**
Cry2-/-	**24.01±0.12 (n=6)**	**26.03±0.58 (n=5)**	**28.14±1.98 (n=136)**	**26.58±0.90 (n=5)**	**28.62±0.58 (n=5)**	**28.79±1.19 (n=20)**
Per+/+	**23.76±0.31 (n=11)**	**24.11±0.44 (n=5)**	**ND**	**23.51±0.34 (n=8)**	**25.84±0.38 (n=6)**	**ND**
Per1-/-	**23.52±0.44 (n=11)**	**24.28±0.77 (n=5)**	**AR/ND (n=12)**	**AR/ND (n=6)**	**AR/ND (n=6)**	**AR/ND (n=1)**
Per2-/-	**22.95±0.30 (n=10)**	**NA**	**NA**	**NA**	**AR [d]**	**ND**
Per3-/-	**23.27±0.18 (n=12)**	**23.78±0.41 (n=5)**	**ND**	**21.98±0.73 (n=6)**	**23.90±0.14 (n=6)**	**ND**

Table S1. Summary of Circadian Period Phenotypes.

Values are presented as mean period (hrs) ± s.d. n: the number of samples (for behavior, explant and fibroblast cultures) or rhythmic samples (for single cells); AR: arrhythmic or unstable rhythm; ND: not determined; NA: not applicable.

(a) The behavioral periods of *Per2-/-* and *Per3-/-* mice were determined elsewhere, and the respective WT control periods in these studies were 23.12 ± 0.11 and 23.77 ± 0.09 (Bae et al., 2001; Shearman et al., 2000).

(b) The periods for *Per1-/-* and *Cry1-/-* individual neurons and fibroblasts could not be determined reliably from the small number of transiently rhythmic cells.

(c) WT lung explants and fibroblast cultures displayed persistent rhythms, but *Per1-/-* and *Cry1-/-* samples showed unstable and less persistent rhythms.

(d) *Per2-/-* fibroblasts were obtained from independent cell lines derived from two mice. Bioluminescence rhythms from the lentiviral *mPer2-dLuc* reporter of at least six dishes per line were monitored.

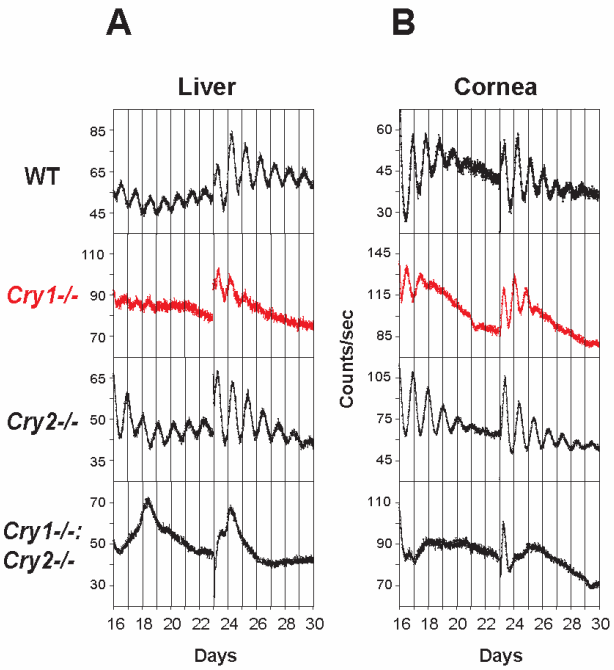

Supplemental Figure S1. *Cry1* Is Required for Sustained Circadian *mPer2*^{Luc} Rhythmicity in Liver and Cornea Explants. Representative records of tissue-autonomous rhythms in liver explants (A) and cornea explants (B) of WT, *Cry1-/-*, *Cry2-/-* and *Cry1-/-:Cry2-/-* knockout mice. Data are shown beginning immediately following a change to fresh EM (day 16), and another medium change occurred at day 23.The liver and cornea explants of WT and *Cry2-/-* mice displayed persistent rhythms, whereas *Cry1-/-* explants were significantly less persistent or largely arrhythmic. Medium change could restart the rhythm, but the revived oscillations were weak and unstable, and were not self-sustained. These results suggest that *Cry1* is indispensable for persistent rhythmicity in the liver and cornea.

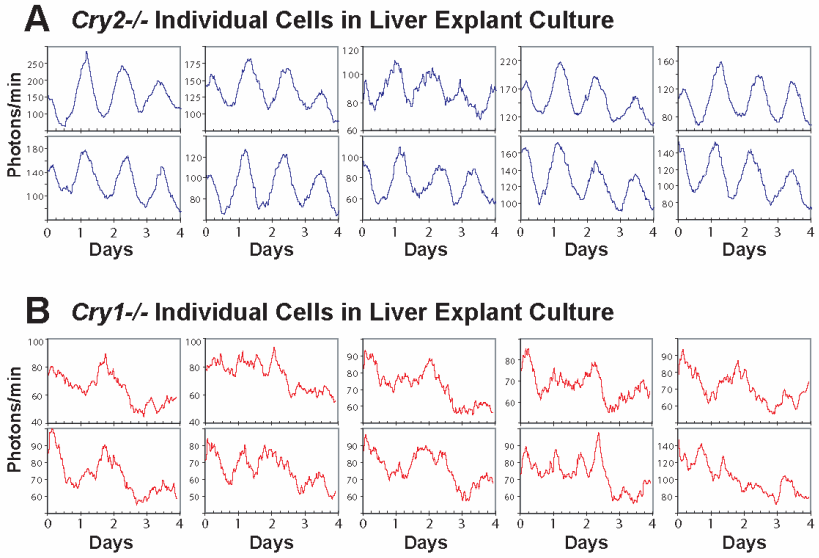

Supplemental Figure S2. *Cry1* Is Required for Sustained Circadian *mPer2*^{Luc} Rhythmicity in Individual Cells of Liver Explants.
Ten representative single cell rhythms from liver explants are presented for (A) *Cry2-/-* and (B) *Cry1-/-* knockout mice. Thin slice cultures (400 μm), prepared and cultured exactly as for SCN slices shown in Figures 6 and 7, were used for single cell imaging. *Cry2-/-* liver cells displayed persistent rhythms. In dramatic contrast, *Cry1-/-* liver cells were arrhythmic. These results show that *Cry1* is required for sustained rhythmicity in liver explants at the single cell level.

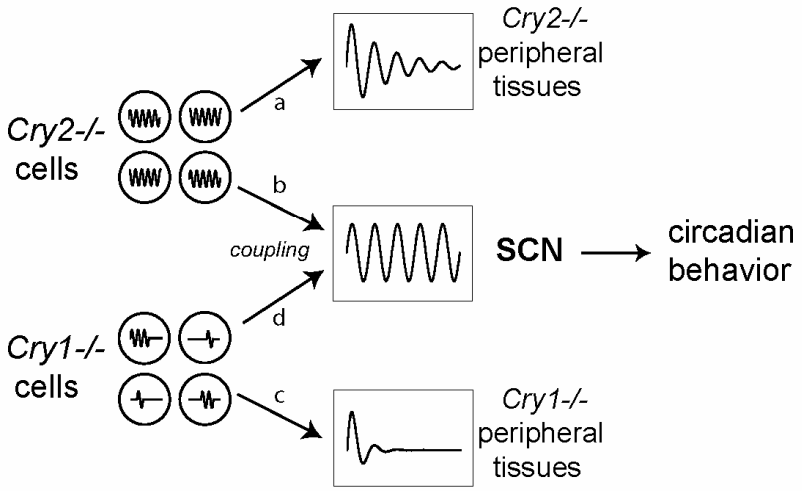

Supplemental Figure S3. Oscillator Network Interactions Provide System Robustness but Mask Cell-Autonomous Phenotypes in Mutant Clock Cells. *Cry2*-deficient individual cells generate persistent circadian oscillations. In peripheral tissue explants (a), where intercellular coupling is absent, these cells can be partly synchronized by various stimuli, but gradually drift out of phase due to differences in circadian period length among cells. This leads to gradual damping of the population rhythm in cell cultures. In SCN slices (b), specialized intercellular coupling keeps cells synchronized, and there is little damping of the population rhythm. In marked contrast to WT and *Cry2-/-* cells, *Cry1*-deficient cells generate only occasional, transient oscillations. In isolated peripheral tissues (c), these oscillations can be briefly synchronized by various stimuli but then rapidly desynchronize and dissipate, leading to arrhythmic patterns of clock gene expression. In SCN slices (d), however, intercellular coupling serves both to stabilize and to synchronize the transient oscillations, leading to robust circadian rhythms at the tissue level. Circadian animal behavior generally reflects the status of the SCN clock, displaying genotype-specific free-running periods. Thus, the strong intercellular coupling uniquely present in the SCN is able to compensate for clock defects in *Cry1-/-* cells, and circadian phenotypes observed in the SCN and from behavior are not cell-autonomous in *Cry1-/-* mice.

Supplemental Experimental Procedures

Lentiviral Clock Reporter Construction

The *dLuc* construct contained a *luciferase* gene and a PEST sequence for rapid protein degradation as previously described (Ueda et al., 2002). The self-inactivating (SIN) lentiviral clock reporter vector contained *dLuc* driven by the *Per2* promoter, extending 526 bp upstream of the transcription start site (Yoo et al., 2005). The promoter DNA fragment was amplified from genomic DNA using a forward primer (CTCGAGCGGATTA CCGAGGCTGGTCACGTC) and a reverse primer (CTCGAGTCCCTTGCTCGGCCCGT CACTTGG). The vector also contained a gene encoding enhanced green fluorescent protein (EGFP), mediated by an internal ribosome entry site (IRES) sequence downstream of *dLuc*, allowing for FACS sorting of cells with integrated vectors. To shield the reporter from integration site effects (Schroder et al., 2002; Brown et al., 2005), an SV40 promoter and terminator (P/T) were introduced immediately upstream of the *mPer2* promoter. Vectors were designed to be self-inactivating (provided by a deletion in the 3'LTR) (Miyoshi et al., 1998) and used the woodchuck hepatitis virus post-transcriptional regulatory element (WPRE) 3' to the transgene (Zufferey et al., 1999). The Rev-response element (RRE) and HIV-1 central poly-purine track (PPT) were located 5' to the *mPer2-dLuc* reporter cassette (Follenzi et al., 2000).

To produce infectious viral particles, HEK293T cells were transfected with lentiviral vector DNA and plasmids encoding accessory factors, i.e. envelope protein, Gag/Pol, and Rev (Naldini et al., 1996; Miyoshi et al., 1998). The culture medium containing the viral particles was harvested 48 hours post transfection and used for subsequent infection of a given cell line. As higher titers of the virus produced greater amplitudes but did not affect the intrinsic period lengths of the fibroblasts of WT controls (data not shown), low titer viral particles were used in this study. Infected primary cells were grown to confluence and directly used for bioluminescence recording. Infected immortalized fibroblasts were propagated and sorted by FACS for EGFP expression to select for reporter positive cells prior to bioluminescence recording. Sorted cells showed increased intensity and improved amplitude.

Serum Shock and Quantitative PCR

For the mRNA time course experiment, spontaneously immortalized fibroblasts were grown to confluence in regular medium. Cells were starved in serum-free medium for 2 hr followed by 50% horse serum treatment. After 2 hr of serum shock, the medium was replaced with serum-free DMEM (time = 0). The first time point for cell harvesting was at 28 hr post serum shock. At the indicated times, the medium was aspirated and immediately replaced with Trizol reagents (Invitrogen), and cells were frozen at -80°C until extraction of total RNA. Duplicate dishes were prepared for each time point, and the time course experiment was repeated twice. One μg of total RNA was used in 20 μl of reverse transcription reaction with the iScript cDNA synthesis kit (BioRad). 100 μl of H_2O was added to each reaction, and 6 μl of the mixture was used in quantitative PCR using an iCycler thermal cycler with the MyiQ optical module (BioRad), as described previously (Sato et al., 2004). Transcript levels for each gene were normalized to *Gapdh*. Average relative expression ratios for each gene were calculated from three

PCR replicates and expressed as a percentage of the maximum ratio at peak expression.

Mathematical Simulation

We employed a previously published mammalian circadian clock computational model (Leloup and Goldbeter, 2003). As the model itself does not differentiate the distinct roles of *Cry1* and *Cry2,* or the differences between the SCN and peripheral oscillators, we used this model not to predict effects of mutations on single cell oscillators, but rather to demonstrate how coupling can compensate for oscillator defects in a network of biophysical oscillators. We first modified the model to mimic the arrhythmic behavior of *Per1-/-* and *Cry1-/-* cellular oscillators. A two-dimensional square grid of individual cells was coupled through *Per* transcription to produce the restoration of robust oscillations observed in SCN tissue explants.

Equations 1-3 detail the conservation equations for *Per* (M_P), *Cry* (M_C), and *Bmal1* (M_B) mRNA. The net rates of accumulation (left hand side) are calculated from the terms on the right hand side that describe transcription rate (v_s), degradation by an enzyme (v_m), and nonspecific degradation added to avoid accumulation (k_{dm}). B_N is the nuclear *Bmal1* concentration, and n and m are the degrees of cooperativity in the Hill expression for the rate of transcription.

$$\frac{dM_P}{dt} = v_{sP}\frac{B_N^n}{K_{AP}^n + B_N^n} - v_{mP}\frac{M_P}{K_{mP} + M_P} - k_{dmp}M_P \qquad (1)$$

$$\frac{dM_C}{dt} = v_{sC}\frac{B_N^n}{K_{AC}^n + B_N^n} - v_{mC}\frac{M_C}{K_{mC} + M_C} - k_{dmc}M_C \qquad (2)$$

$$\frac{dM_B}{dt} = v_{sB}\frac{K_{IB}^m}{K_{IB}^m + B_N^m} - v_{mB}\frac{M_B}{K_{mB} + M_B} - k_{dmb}M_B\,. \qquad (3)$$

The arrhythmic behavior of the individual *Per1-/-* and *Cry1-/-* neurons was reproduced in the mathematical model by introducing noise to the *Bmal1* degradation rate v_{mB} (equation 3) and the activation threshold K_{AC} (equation 2) of nuclear BMAL1 on *Cry* transcription, to yield a stochastic differential equation (SDE) model. SDE models have found application in biological systems that have large numbers of molecules, but exhibit significant fluctuations. The mean values of v_{mB} and K_{AC} were chosen to reproduce the damped oscillation result in the absence of noise (Figure 7A in (Leloup and Goldbeter, 2003). All other parameters were set to the basal values. Simulations were run with different levels of Gaussian noise, with standard deviation (σ) ranging from 0% to 70% of the mean value. As the noise level increased, the cells became less rhythmic. Gaussian noise with a standard deviation of 40% ($\sigma = 0.4$) produced the best match in rhythmicity between the modeled PER protein concentrations and the *Per1-/-* and *Cry1-/-* SCN neuron measurements shown in Figure 5. To demonstrate the effect of coupling on these arrhythmic oscillators, a simple coupling mechanism was introduced, making the *Per* transcription rate dependent on the *Per* mRNA concentration in the surrounding cells, weighted by their proximity. In the originally published model, *Per* transcription rate was modulated to enable entrainment of the oscillator to light/dark cycles (Leloup and Goldbeter, 2003), so it was a logical candidate for a simple coupling

mechanism. The basal *Per* transcription rate v_{sP} was replaced by the coupled rate v_{sPc} where

$$v_{sPc_i} = v_{sP} + CBT\frac{\gamma_i}{KC + \gamma_i} \quad (4)$$

$$\gamma_i = \frac{1}{2}M_{Pi} + \frac{1}{2}\sum_{j=1,j\neq i}^{n}\frac{M_{Pj}}{r_{i,j}} \quad (5)$$

v_{sPci} is the *Per* mRNA transcription rate of the *i*th cell. The coupling strength CBT was set equal to the basal transcription rate, v_{sP} = 1.1, and the Hill type activation threshold KC = 0.3. M_{Pj} is the *Per* mRNA concentration in the *j*th cell, and $r_{i,j}$ is the distance between the *i*th and *j*th cells. A grid of 10x10 cells is considered, so n = 100. The results of coupling the arrhythmic oscillators for σ = 0.4 in a 10x10 grid are shown in Figure 7. Robust oscillation was also restored for σ = 0.5 and σ = 0.6 noise levels with some variation in magnitude associated with the addition of noise into the model. At the larger noise level of σ = 0.7, rhythmicity began to deteriorate in the coupled 10x10 grid, suggesting a noise range over which coupling was effective. These simulation results reinforce the experimental measurements that point to intercellular coupling as the key to sustaining robust oscillations in the SCN.

Supplemental Movie Legends

Movie S1. Dissociated *Cry2-/-* SCN Neurons Are Rhythmic.
A time-lapse bioluminescence movie of dissociated *Cry2-/-* SCN neurons throughout the course of a 7 day experiment (see Supplementary Methods). The field of view is ~3 mm wide. Note the prominent circadian oscillations of bioluminescence intensity (~6 cycles in 7 days, reflecting a mean ~28 hr period), and that rhythms are not synchronized among individual cells.

Movie S2. Dissociated *Cry1-/-* SCN Neurons Are Arrhythmic.
A time-lapse bioluminescence movie of dissociated *Cry1-/-* SCN neurons throughout the course of a 7 day experiment, using procedures identical to those for Movie S1. Note the absence of prominent circadian oscillations. Some cells move during the experiment, and some show an abrupt cessation of luminescence representing cell death at ~2 days, but the majority show persistent, fairly constant levels of bioluminescence, in contrast to the prominent rhythms of WT and *Cry2-/-* neurons.

Supplemental References

Bae,K., Jin,X.W., Maywood,E.S., Hastings,M.H., Reppert,S.M., and Weaver,D.R. (2001). Differential functions of mPer1, mPer2, and mPer3 in the SCN circadian clock. Neuron *30*, 525-536.

Brown,S.A., Fleury-Olela,F., Nagoshi,E., Hauser,C., Juge,C., Meier,C.A., Chicheportiche,R., Dayer,J.M., Albrecht,U., and Schibler,U. (2005). The period length of fibroblast circadian gene expression varies widely among human individuals. PLoS. Biol. *3*, e338.

Follenzi,A., Ailles,L.E., Bakovic,S., Geuna,M., and Naldini,L. (2000). Gene transfer by lentiviral vectors is limited by nuclear translocation and rescued by HIV-1 pol sequences. Nat. Genet. *25*, 217-222.

Leloup,J.C. and Goldbeter,A. (2003). Toward a detailed computational model for the mammalian circadian clock. Proc. Natl. Acad. Sci. U. S. A. *100*, 7051-7056.

Miyoshi,H., Blomer,U., Takahashi,M., Gage,F.H., and Verma,I.M. (1998). Development of a self-inactivating lentivirus vector. J. Virol. *72*, 8150-8157.

Naldini,L., Blomer,U., Gallay,P., Ory,D., Mulligan,R., Gage,F.H., Verma,I.M., and Trono,D. (1996). In vivo gene delivery and stable transduction of nondividing cells by a lentiviral vector. Science *272*, 263-267.

Sato,T.K., Panda,S., Miraglia,L.J., Reyes,T.M., Rudic,R.D., McNamara,P., Naik,K.A., FitzGerald,G.A., Kay,S.A., and Hogenesch,J.B. (2004). A functional genomics strategy reveals Rora as a component of the mammalian circadian clock. Neuron *43*, 527-537.

Schroder,A.R., Shinn,P., Chen,H., Berry,C., Ecker,J.R., and Bushman,F. (2002). HIV-1 integration in the human genome favors active genes and local hotspots. Cell *110*, 521-529.

Shearman,L.P., Jin,X.W., Lee,C.G., Reppert,S.M., and Weaver,D.R. (2000). Targeted disruption of the mPer3 gene: Subtle effects on circadian clock function. Mol Cell Biol *20*, 6269-6275.

Ueda,H.R., Chen,W.B., Adachi,A., Wakamatsu,H., Hayashi,S., Takasugi,T., Nagano,M., Nakahama,K., Suzuki,Y., Sugano,S., Iino,M., Shigeyoshi,Y., and Hashimoto,S. (2002). A transcription factor response element for gene expression during circadian night. Nature *418*, 534-539.

Yoo,S.H., Ko,C.H., Lowrey,P.L., Buhr,E.D., Song,E.J., Chang,S., Yoo,O.J., Yamazaki,S., Lee,C., and Takahashi,J.S. (2005). A noncanonical E-box enhancer drives mouse Period2 circadian oscillations in vivo. Proc. Natl. Acad. Sci. U. S. A. *102*, 2608-2613.

Zufferey,R., Donello,J.E., Trono,D., and Hope,T.J. (1999). Woodchuck hepatitis virus posttranscriptional regulatory element enhances expression of transgenes delivered by retroviral vectors. J. Virol. *73*, 2886-2892.